Doping effect on the electronic structure and thermodynamic properties in $Ce_3Ru_4Sn_{13}$

L. Kalinowski,[1] J. Goraus,[1] P. Witas,[1] and A. Ślebarski[1,2]

[1]*Institute of Physics, University of Silesia, Uniwersytecka 4, 40-007 Katowice, Poland*

[2]*Centre for Advanced Materials and Smart Structures, Polish Academy of Sciences, Okólna 2, 50-950 Wrocław, Poland*

(Received 19 September 2016; revised manuscript received 7 November 2016; published 27 December 2016)

A comprehensive study of heat and electric transport, magnetic, and electronic structure (experiment and calculations) properties is reported for a skutterudite-related $Ce_3Ru_4Sn_{13}$ heavy fermion system with the respective substitution of Co and Sb into Ru and Sn sites. $Ce_3Ru_4Sn_{13}$ is obtained as a heavy fermion system with high electronic contribution to the specific heat $C(T)/T$ of $\sim$3 J/K^2 mol$_{Ce}$, and a significant Schottky anomaly below about 10 K. The complex study gives a consistent interpretation of the impact of doping on the crystal electric-field effect and Kondo temperature. For $Ce_3Ru_4Sn_{13}$ we report a field-induced phase transition between the magnetically correlated heavy fermion phase and the single-ion Kondo impurity state, which does not depend on the type of dopant. We also demonstrate that doping does not improve the poor thermoelectric properties of $Ce_3Ru_4Sn_{13}$.

DOI: 10.1103/PhysRevB.94.235151

I. INTRODUCTION

Ternary filled skutterudites RM_4X_{12} with rare earth R, d-electron metal M, and a pnictogen element X (P, As, or Sb) have attracted much interest because of a variety of ground states including strongly correlated superconducting behaviors, and because of their large thermoelectric potential. A wide variety of these interesting behaviors results from subtle interplay between magnetic and Kondo interactions [1]. In the critical regime known as a quantum critical point (QCP), magnetic ordering and Kondo interaction compensate, therefore the system is at the threshold of an instability and even weak perturbations, e.g., disorder [2] or structural instability [3], can cause significant effects by changing the nature of the quantum macrostate.

Skutterudite-related stannides with stoichiometry $Ce_3M_4Sn_{13}$ have received renewed attention (i) because of a possible presence of QCP [4–6]; (ii) because the La-reference compounds are proving to be interesting in the context of nanoscale electronic disorder, which is responsible for an increase in superconducting critical temperature T_c [2]; (iii) because $Sr_3Rh_4Sn_{13}$ revealed an existence of a novel structural quantum phase transition [7]; and (iv) because of the impact of d-electron-type correaltions on their electronic structure [8].

A remarkable feature of the $Ce_3M_4Sn_{13}$ system is its tunable nature (see [9]). This offers an opportunity to investigate the impact of the change of the number of the conduction electrons in the parent system, e.g., $Ce_3Ru_4Sn_{13}$, by partial replacement of Sn by Sb or Ru by Co, and/or the effect of an applied magnetic field on its ground-state properties. In this work we report complex measurements and calculations of the electronic structure, heat and electron transport, and thermodynamic properties of $Ce_3Ru_4Sn_{13}$; we also discuss the impact of doping on its ground-state properties. Our comprehensive study (experiment and calculations) documented for $Ce_3Ru_4Sn_{13}$ a field-induced transition between a low-field magnetically correlated Kondo lattice state and a single-ion Kondo impurity state observed at the applied magnetic fields $B >\sim 2.5$ T.

While some of the ternary skutterudites RM_4X_{12} exhibit well-evidenced thermoelectric properties (e.g., [10]), in contrast the $Ce_3M_4Sn_{13}$ clathrates are not yet thoroughly examined. The significant thermopower of these strongly correlated compounds has been expected due to the high gradient of the density of states (DOS) at the Fermi level ($S \sim \frac{dN(E)}{dE}$, where S is the Seebeck coefficient) as a result of Kondo resonance, and the cage-type structure. Therefore, the aim of this work is also to evaluate thermoelectric properties of $Ce_3Ru_4Sn_{13}$ doped with Co or Sb. Special emphasis is addressed to crystal electric-field (CEF) splitting, which determines low-temperature magnetic and transport properties.

II. EXPERIMENTAL DETAILS

The samples were prepared by arc melting technique. Spectrally pure elements with stoichiometric mass ratio were remelted several times on a water cooled cooper heart at high purity argon atmosphere with an Al getter. To ensure homogeneity and purity, the samples were annealed at 870°C for 2 weeks. All samples were examined by x-ray-diffraction (XRD) analysis and found to have a cubic structure (space group $Pm\bar{3}n$) [11]. Figure 1 shows representative diffraction patterns with Rietveld refinements. The lattice parameters of $Ce_3Ru_xCo_{4-x}Sn_{13}$ and $Ce_3Ru_4Sn_{13-x}Sb_x$ shown in the inset to the figure increase with doping, which suggests that the samples are stoichiometric.

Stoichiometry and homogeneity were checked by the microprobe technique and by x-ray photoelectron spectroscopy (XPS) analysis. Deviations from the nominal composition were small.

The XPS spectra were obtained with monochromatized Al K_α radiation at room temperature using a PHI 5700 ESCA spectrometer. Each polycrystalline sample was broken under high vacuum better than 6×10^{-10} Torr immediately before taking a spectrum.

Electrical resistivity ρ at ambient pressure was investigated by a conventional four-point ac technique using a Quantum Design Physical Properties Measurement System (PPMS). The PPMS platform was used for thermal conductivity, thermopower, and resistivity measurements in the temperature range $\sim$2–300 K.

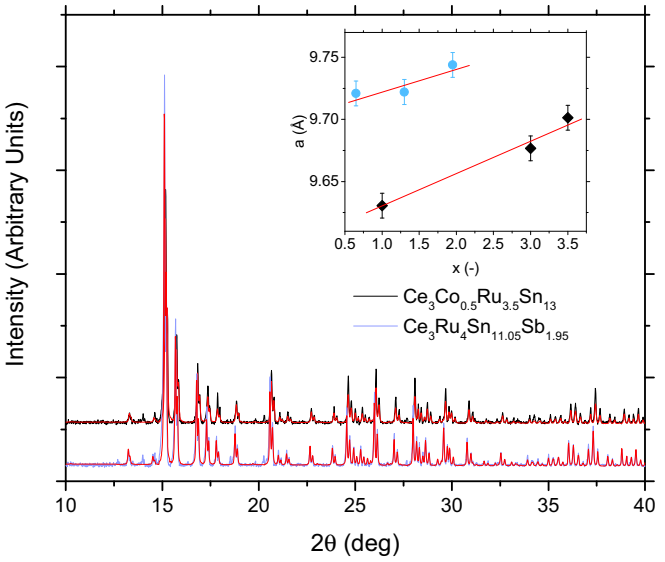

FIG. 1. XRD patterns with Mo K_α radiation for $Ce_3Co_{0.5}Ru_{3.5}Sn_{13}$ (black line) and $Ce_3Ru_4Sn_{11.05}Sb_{1.95}$ (blue line) with Rietveld refinement (red line). Inset displays the lattice parameter a vs x for $Ce_3Ru_4Sn_{13-x}Sb_x$ (blue points) and $Ce_3Ru_xCo_{4-x}Sn_{13}$ (black points).

Specific heat C was measured in the temperature range 0.4–300 K and in external magnetic fields up to 6 T using a Quantum Design PPMS platform. The dc magnetization M and magnetic susceptibility χ were obtained using a commercial superconducting quantum interference device magnetometer from 1.8 to 300 K in magnetic fields up to 7 T.

The band-structure calculations were accomplished using fully relativistic full potential local orbital method (FPLO9-00-34 computer code [12]), as well as augmented plane-wave local orbital method [13]. Doping of Sb in $Ce_3Ru_4Sn_{13-x}Sb_x$ and Ru atoms in $Ce_3Ru_xCo_{4-x}Sn_{13}$ was studied within the virtual crystal approximation, using the supercell approach. The exchange correlation potential V_{xc} was used in the form proposed by Perdew and Wang [14] in both cases. The number of k points in the irreducible wedge of the Brillouin zone was 80.

III. RESULTS AND DISCUSSION

A. Electronic structure: Experiment and calculations

In previous works [6,8,15–17] we discussed in detail the electronic structure at ambient and external pressure of the stannide family $R_3M_4Sn_{13}$, where R = Ce, La and M = Co, Rh, Ru. The goal of this work is to show the impact of the change in the number of valence electrons of the $Ce_3Ru_4Sn_{13}$ parent compound on its electronic structure and physical properties. In order to explain the alloying effect on the band-structure character, we analyze core-level and valence-band (VB) XPS spectra of $Ce_3Ru_4Sn_{13}$ partially substituted by Co or Sb, respectively. Figure 2 shows VB XPS spectra of different $Ce_3(Ru,Co)_4Sn_{13}$ and $Ce_3Ru_4(Sn,Sb)_{13}$ alloys, and the calculated total DOSs of $Ce_3Co_4Sn_{13}$ and $Ce_3Ru_4Sn_{11.05}Sb_{1.95}$. The spectra $a-g$ are very similar and dominated by the metal M $3d$ or $4d$ states (see Fig. 3). The broad maximum centered at ~7 eV is related to Sn(Sb) $5s$ states. With doping

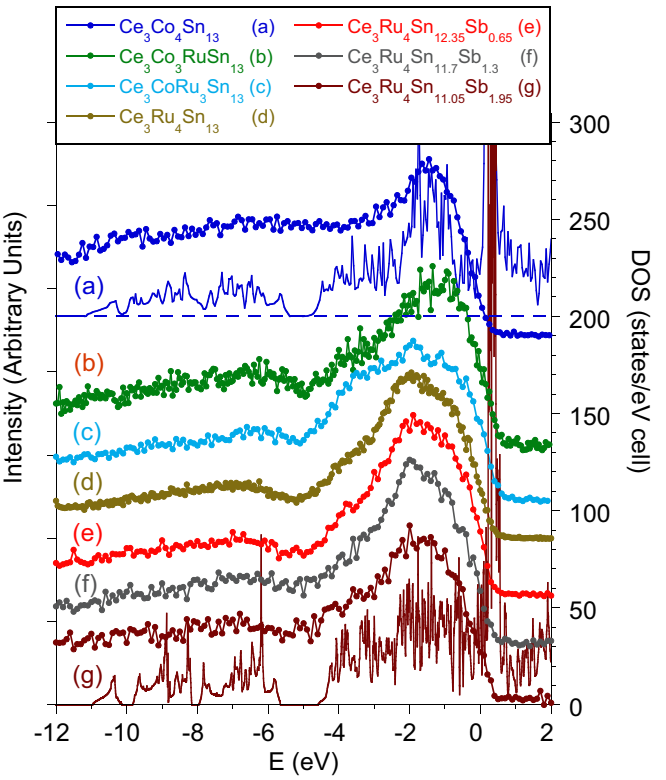

FIG. 2. Valence-band XPS spectra for the samples labeled at the top of the figure. Also are shown the total DOS calculated for $Ce_3Co_4Sn_{13}$ (a), and $Ce_3Ru_4Sn_{11.05}Sb_{1.95}$ (g).

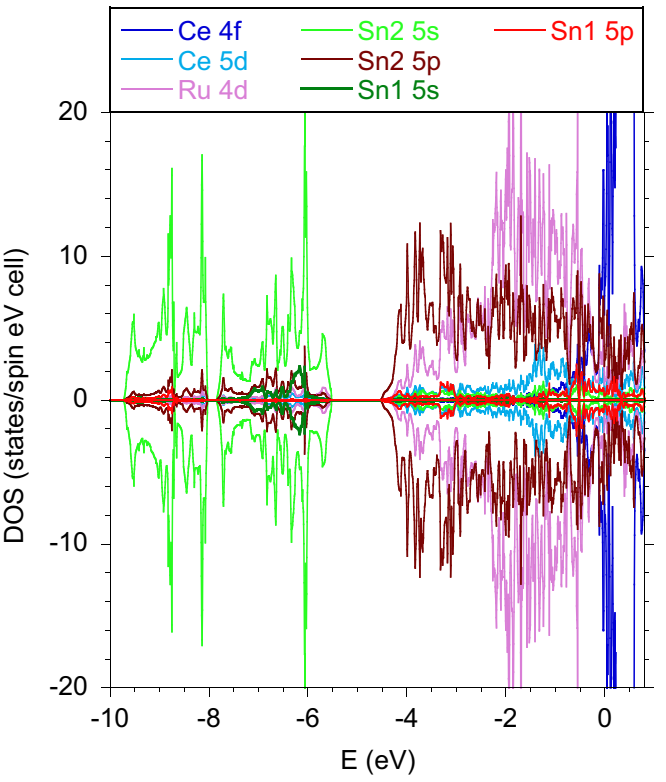

FIG. 3. Atomic partial DOS for $Ce_3Ru_4Sn_{11.05}Sb_{1.95}$.

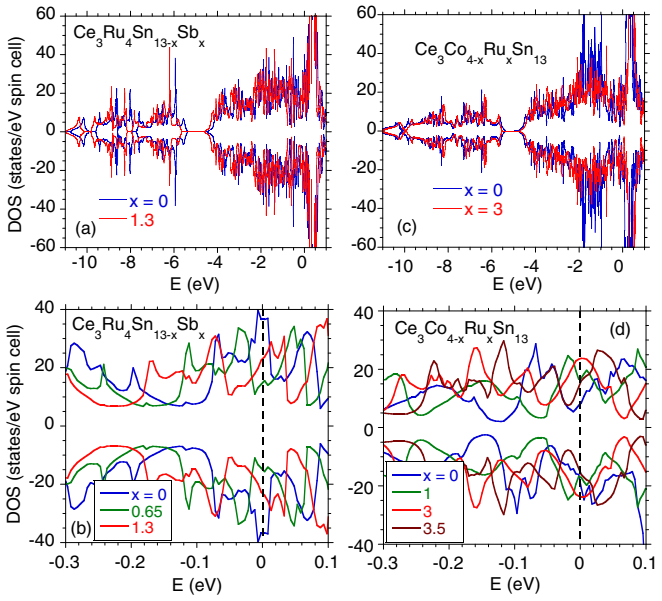

FIG. 4. Effect of Sb doping in $Ce_3Ru_4Sn_{13-x}Sb_x$ (a) and of Ru doping in $Ce_3Ru_xCo_{4-x}Sn_{13}$ (c) on the total DOS. Panels (b) and (c) exhibit total DOSs near the Fermi level in detail.

of Sb the bands slightly shift to higher bonding energy, which does not change the shape of the XPS spectra, but strongly determines the total DOS at the Fermi level, as shown in Fig. 4 (will be discussed). Figure 5 displays the minority- and majority-spin Fermi-surface (FS) sheets in the first Brillouin zone for the system of $Ce_3Ru_xCo_{4-x}Sn_{13}$ compounds. The spin-down and spin-up FS sheets are for $Ce_3Co_4Sn_{13}$ slightly different, which indicates its magnetic instability when the long-range magnetic order is experimentally excluded down to 0.35 K [5]; for the remaining $Ce_3Ru_xCo_{4-x}Sn_{13}$ compounds both spin-polarized Fermi surfaces are identical. The topology of the FS of the samples $x = 1$, 3, and 3.5 may favor nesting and enhance the Pauli susceptibility (see Sec. III B).

Figure 6 shows the Ce $3d$ core-level XPS spectra. The separation of the overlapping peaks is shown as an example for the sample $Ce_3Ru_4Sn_{11.7}Sb_{1.3}$. The main components $3d^9_{5/2}4f^1$ and $3d^9_{3/2}4f^1$ exhibit a spin-orbit (SO) splitting, while the presence of $3d^94f^2$ SO components results from the intra-atomic hybridization between the $4f$ electrons and conduction band. From the intensity ratio $I(f^1)/[I(f^1) + I(f^2)]$ one can estimate hybridization energy Δ_{cf} on the basis of the method proposed by Gunnarsson and Schönhammer [18] with the accuracy of about 20%. For details we refer to [19]. Energy $\Delta_{cf} = \pi V_{cf}^2 N(\epsilon_F)$ expresses the hybridization part of the Anderson impurity Hamiltonian [20], and V_{cf} is the hybridization matrix element. The high-energy $3d^9_{5/2}4f^0$ and $3d^9_{3/2}4f^0$ components about 11 eV away from the main $3d^94f^1$ peaks are not observed in the spectra, which confirms almost localized character of the $4f$ states. A stable Ce^{3+} configuration is also supported by the Ce $4d$ XPS core-level spectra shown in Fig. 7, which do not exhibit satellite peaks at binding energies of about 118–124 eV (for details, see [21]). The high-energy XPS d-electron spectra confirm the stable $4f^1$ configuration of the f-electron shell, and relatively small hybridization

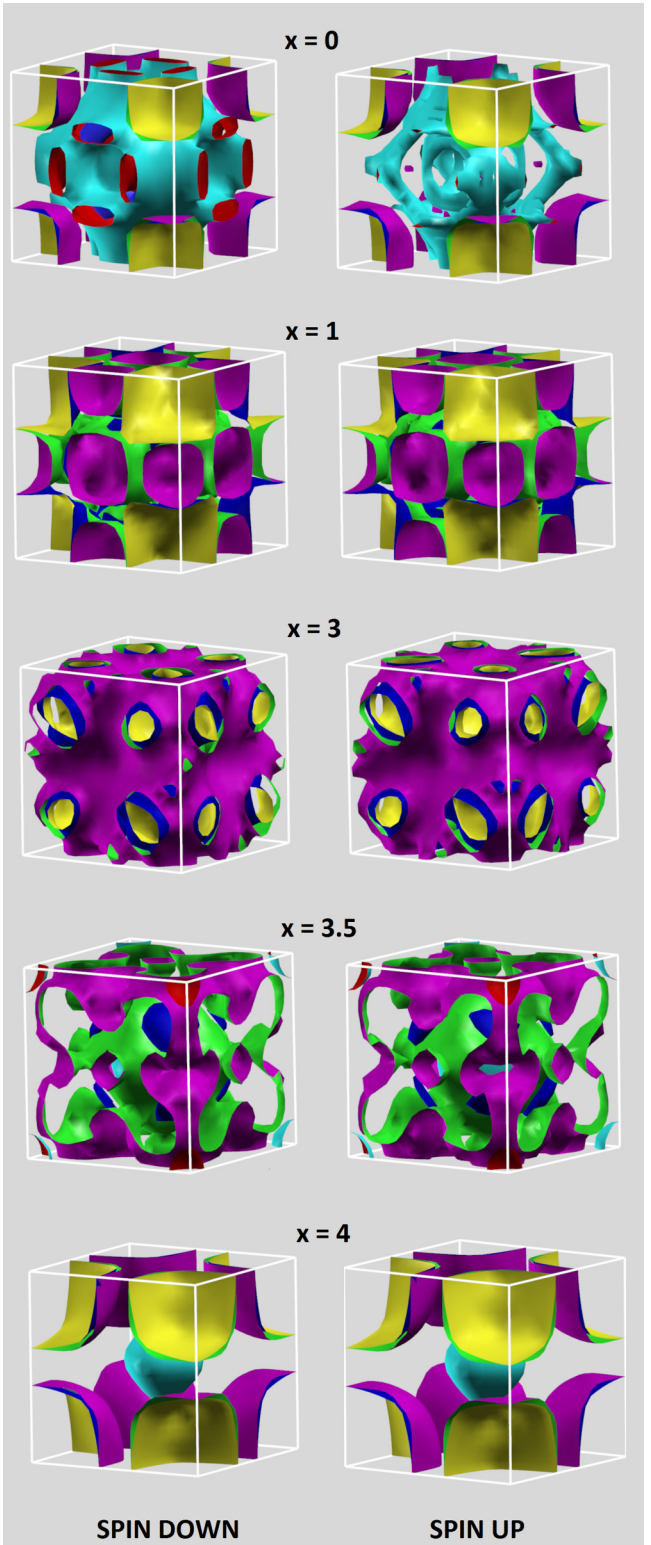

FIG. 5. The Fermi-surface sheets of $Ce_3Co_{4-x}Ru_xSn_{13}$ in the first Brillouin zone. Left column corresponds to the spin down; right column corresponds to spin up. The Γ point is at the center of the cubic Brillouin zone. The calculations were carried out for the high-temperature structure $Pm\bar{3}n$.

energy $\Delta_{cf} \approx 70$–90 meV for $Ce_3Ru_4Sn_{13-x}Sb_x$, and larger $\sim$110 meV for $Ce_3Ru_{4-x}Co_xSn_{13}$. In Table I we summarize the data which allowed us to calculate the coupling constant

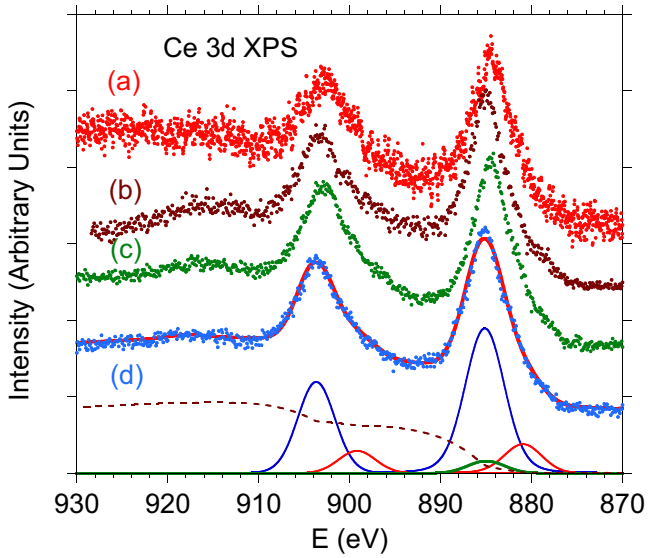

FIG. 6. The Ce $3d$ XPS spectra at room temperature for $Ce_3Co_4Sn_{13}$ (a), $Ce_3RuCo_3Sn_{13}$ (b), $Ce_3Ru_4Sn_{13}$ (c), and $Ce_3Ru_4Sn_{11.7}Sb_{1.3}$ (d), and as an example, a deconvoluted spectrum for $Ce_3Ru_4Sn_{11.7}Sb_{1.3}$ on the basis of the Gunnarsson-Schönhammer theoretical model, with spin-orbit components $3d^9 4f^1$ (blue line) and $3d^9 4f^2$ (red line). The brown dotted line represents the background; the thick red line shows the fit after deconvolution to the lowest XPS spectrum. From the deconvolution procedure, the Sn $3s$ line contribution at 885 eV (green line) provides about 15% of the total peak intensity due to $3d^9_{5/2} 4f^1$ final states.

$J_{cf} = \frac{2V_{cf}^2}{|\epsilon_f - \epsilon_F|}$ [22]. As shown in Table I only a small amount of the Sb impurity can lead to stronger Kondo coupling, while for larger concentration of Sb J_{cf} is equal to that in the parent $Ce_3Ru_4Sn_{13}$ sample. For $Ce_3Co_4Sn_{13}$ doped with Ru the coupling $J_{cf} \approx 30$ meV has a similar value.

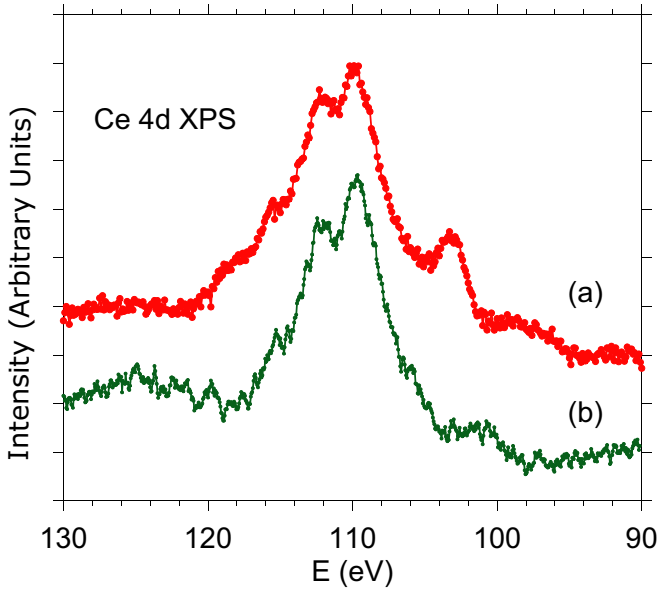

FIG. 7. The Ce $4d$ XPS spectra for $Ce_3Ru_4Sn_{11.05}Sb_{1.95}$ (a) and $Ce_3Ru_3CoSn_{13}$ (b) with no evidence of the $4d^9 4f^0$ components.

TABLE I. Energy Δ_{cf}, the total density of states $N(\epsilon_F)$ at the Fermi level, hybridization matrix element V_{cf}, energy of the maxima of f-electron states in relation to the Fermi level, and J_{cf} interaction between the f-electron states and the conduction-band states.

x	Δ_{cf} (meV)	$N(\epsilon_F)$ (eV^{-1} f.u.$^{-1}$)	V_{cf} (meV)	$\lvert\epsilon_f - \epsilon_F\rvert$ (eV)	J_{cf} (meV)
		$Ce_3Ru_4Sn_{13-x}Sb_x$			
0	70	36.2	24.8	0.045	27.3
0.65	85	14.5	42.5	0.032	81.2
1.3	80	23.1	33.3	0.07	31.7
1.95	90	23.1	35.2	0.07	35.4
		$Ce_3Ru_xCo_{4-x}Sn_{13}$			
0	140	14.3	55.8	0.08	77.9
1	110	16.9	45.5	0.13	32.0
3	110	23.7	38.4	0.08	34.7

Figure 8 shows the Sn $4d$ XPS spectra. The reason is as follows: recently [15] we suggested that the asymmetry of the Sn $4d$ spectrum may be associated with the change of local symmetry of the Sn2 cage due to strong covalent bonding between metal M and Sn2. In effect of deformation of the $(Sn2)_{12}$ cages, the local CEF symmetry of the Ce ion in $Ce_3M_4Sn_{13}$ is not cubic but lower. We found similar asymmetry of the Sn $4d$ lines for all the components of the $Ce_3Ru_4Sn_{13-x}Sb_x$ system, while increasing the Co substitution in the Ru sites makes the effect more pronounced. We therefore suspect similar CEF splitting for the family of the $Ce_3Ru_4Sn_{13-x}Sb_x$ compounds and much stronger CEF effect for $Ce_3Ru_{4-x}Co_xSn_{13}$, which will be discussed in Sec. III B

B. Magnetic properties of Sb- and Co-doped $Ce_3Ru_4Sn_{13}$

The XPS results are related to the following consequences.

(i) The stable configuration of the Ce $4f$ shell and weak hybridization energy Δ_{cf} indicates a single-ion Kondo behavior in the both nonmagnetic $Ce_3Ru_4Sn_{13-x}Sb_x$ and $Ce_3Ru_{4-x}Co_xSn_{13}$ systems.

(ii) The covalent bonding between Ru and Sn2 atoms (cf. Sn $4d$ XPS spectra shown in Fig. 8) leads to deformation of the Sn_{12} cages, which leads to lower local symmetry of CEF of Ce^{3+} ions. Similar behavior has been reported for other $R_3M_4Sn_{13}$ compounds [6,8,17]. On the basis of these assumptions we will interpret magnetic properties.

Figure 9(c) shows the magnetization M versus B isotherms for $Ce_3Ru_4Sn_{11.7}Sb_{1.3}$. They are well approximated by the Langevin function $L(\xi) = \coth(\xi) - 1/\xi$, where $\xi = \mu B/k_B T$ with total magnetic moment $\mu = 0.9\ \mu_B$ (obtained for the isotherm at $T = 2$ K). The magnetization does not show any hysteresis in the field dependence of M. The same $M(B)$ behavior was observed for the remaining $Ce_3Ru_4Sn_{13-x}Sb_x$ and $Ce_3Ru_{4-x}Co_xSn_{13}$ samples (we noted for $Ce_3Ru_{4-x}Co_xSn_{13}$ with $x \geqslant 3$ smaller value of $\mu \approx 0.7\ \mu_B$; the reason may be a large χ_0 value and the associated screening effect). Figure 9(a) shows the temperature dependence of the dc magnetic susceptibility, $\chi(T)$, and inverse susceptibility data, $1/\chi$, for $Ce_3Ru_4Sn_{13-x}Sb_x$ ($x = 0.65$ and 1.3). The experimental $1/\chi(T)$ data are well approximated by the CEF model considering the tetragonal Ce point symmetry,

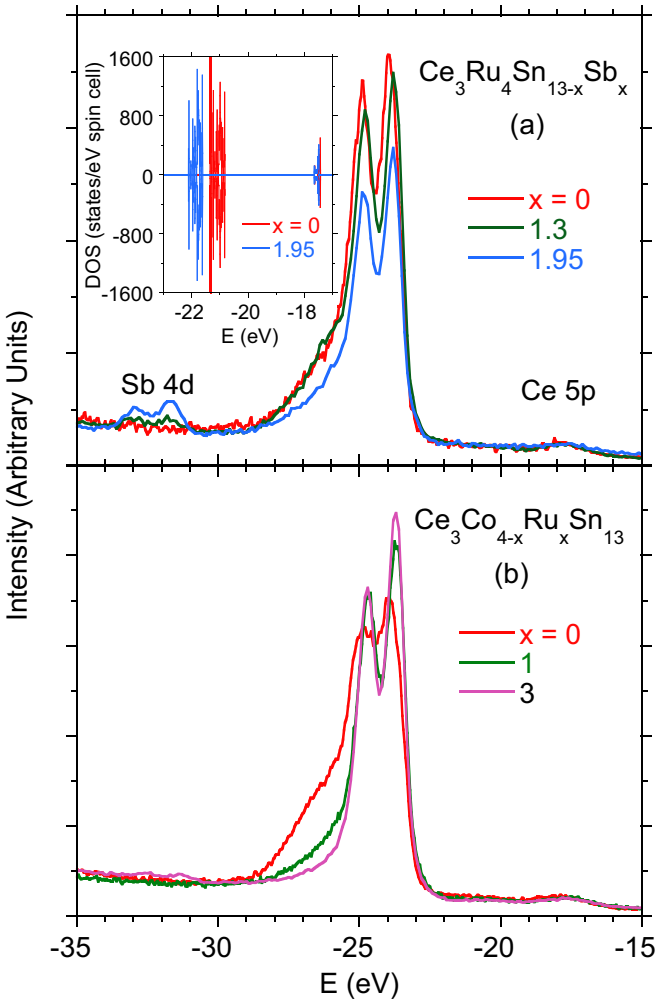

FIG. 8. The Sn 4*d* XPS spectra for $Ce_3Ru_4Sn_{13-x}Sb_x$ (a) and for $Ce_3Ru_{4-x}Co_xSn_{13}$ (b). The inset shows the calculated Sn 4*d* DOS. Note, the intensity of the Sb 4*d* line increases with increasing amount of Sb, as expected.

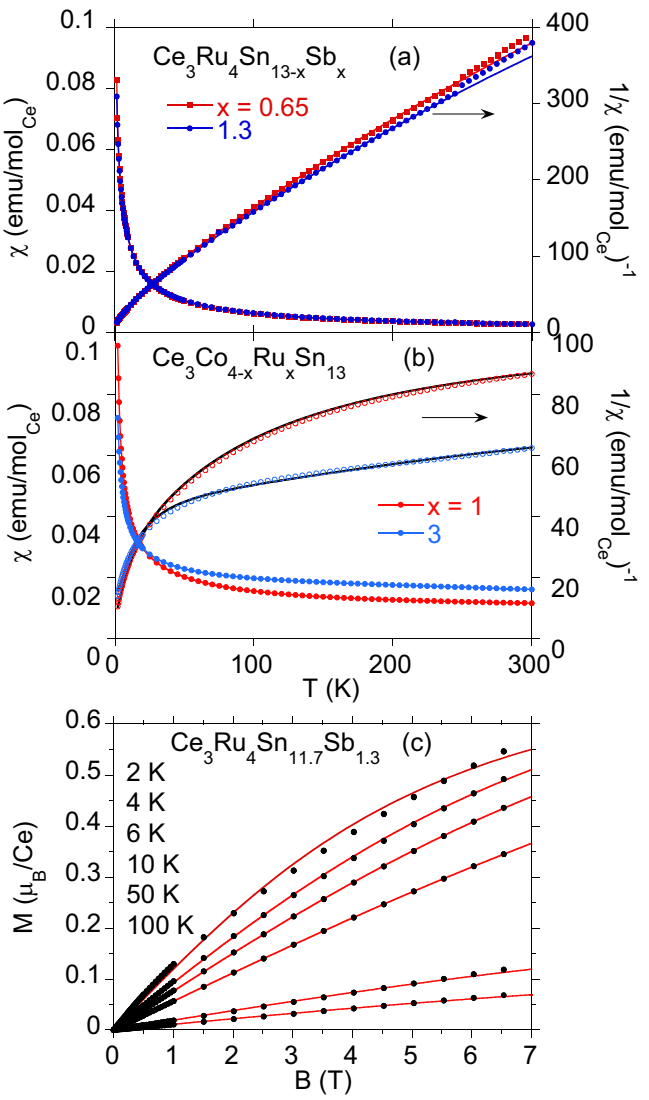

FIG. 9. (a) Magnetic susceptibility χ of $Ce_3Ru_4Sn_{13-x}Sb_x$ in external field of 1000 Gs. The solid red line represents the CEF fit to $1/\chi$ data for the two excited doublets separated from the ground-state doublet by energy $\Delta_1 = 12$ K for $x = 0.65$ and 11 K for $x = 1.3$, and $\Delta_2 = 117$ K ($x = 0.65$) and 110 K ($x = 1.3$), respectively. The deviation of $1/\chi$ from the fit observed above ~200 K is due to structural deformation (see [15]). In panel (b) the Van Vleck formula is fitted to χ and $1/\chi$ data measured at magnetic field of 1000 Gs for the $Ce_3Ru_xCo_{4-x}Sn_{13}$ samples. The total CEF splitting of two doublets is about 245 K for sample $x = 1$, 470 K for sample $x = 3$, and 500 K for sample $x = 3.5$. Panel (c) displays magnetization M per Ce atom vs magnetic field B measured at different temperatures for $Ce_3Ru_4Sn_{11.7}Sb_{1.3}$. The solid lines are fits of the Langevin function to the magnetization data. Very similar M vs B isoterms are obtained for remaining compounds.

where the $J = 5/2$ multiplet of the Ce^{3+} ion splits into three doublets separated from the ground state by energies $\Delta_1 \approx 11$ K and $\Delta_2 \approx 110$ K, respectively. The Van Vleck fitting formula supplemented by the temperature-independent Pauli contribution χ_0 takes the form [23]

$$\chi_{\mathrm{CEF}} = \frac{N_A \mu_B^2}{k_B} \frac{\sum_i \left(\frac{a_i}{T} + b_i\right) \exp\left(\frac{-\Delta_i}{k_B T}\right)}{\sum_i \exp\left(\frac{-\Delta_i}{k_B T}\right)} + \chi_0, \qquad (1)$$

where summations run over all i states of energies E_i and $\Delta_i = E_i - E_0$, N_A is the Avogadro number, k_B is a Boltzman constant, and $\chi_0 \approx 6 \times 10^{-4}$ emu/mol$_{\mathrm{Ce}}$. Figure 9(b) shows $\chi(T)$, and inverse susceptibility data, $1/\chi$, for $Ce_3Co_3RuSn_{13}$. Very similar $\chi(T)$ plots were obtained for remaining $Ce_3Ru_{4-x}Co_xSn_{13}$ compounds, however, we noted different splitting of the $J = 5/2$ multiplet in the series than the respective crystal-field level scheme of $Ce_3Ru_4Sn_{13-x}Sb_x$ samples. Namely, for sample $x = 1$, $\Delta_1 = 10$ K, $\Delta_2 = 245$ K; for $x = 3$ $\Delta_1 = 13.5$ K, $\Delta_2 = 471$ K; and for $x = 3.5$ $\Delta_1 = 11.5$ K, $\Delta_2 = 500$ K, and $\chi_0 \approx 5 \times 10^{-3}$ emu/mol$_{\mathrm{Ce}}$.

The χ_0 value for $Ce_3Co_4Sn_{13}$ doped with Ru is one order of magnitude larger than that obtained for $Ce_3Ru_4Sn_{13-x}Sb_x$ alloys. Considering the similar values of $N(\epsilon_F)$ and J_{cf} (see Table I) for both series; the larger χ_0 signals here have stronger correlation effect and/or topology of the Fermi surface.

Figures 10 and 11 display the low-temperature specific heat of $Ce_3Ru_4Sn_{12.35}Sb_{0.65}$ and $Ce_3Co_3RuSn_{13}$, respectively,

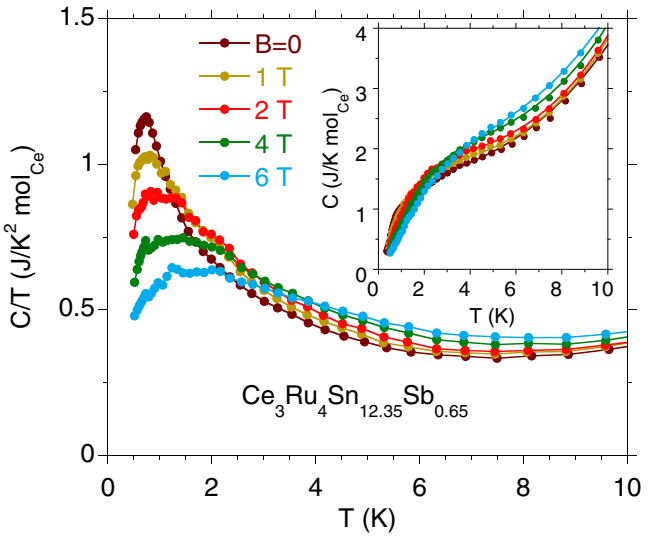

FIG. 10. $C(T)/T$ vs T for $Ce_3Ru_4Sn_{12.35}Sb_{0.65}$. The inset shows $C(T)$ data and the fit of the resonance level model to the experimental data.

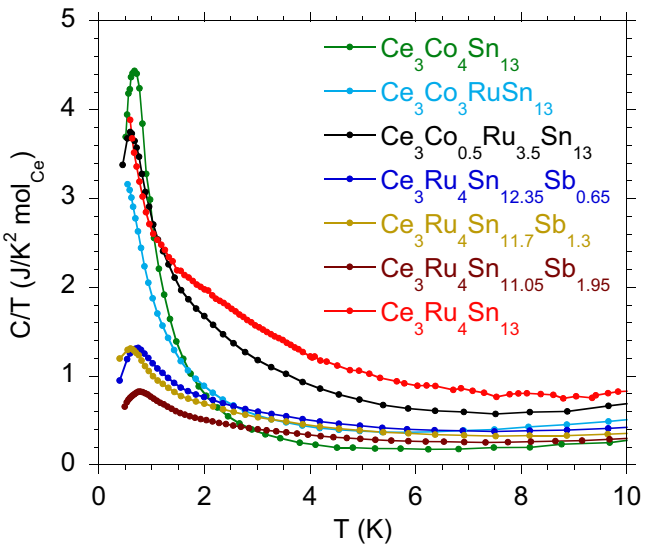

FIG. 12. $C(T)/T$ vs T ($B = 0$) for different $Ce_3Ru_4Sn_{13-x}Sb_x$ and $Ce_3Co_{4-x}Ru_xSn_{13}$ samples.

as $C(T)/T$. Figure 12 compares the $C(T)/T$ data at $B = 0$ for all investigated samples. The large value of $C(T)/T \approx 4$ J/K^2 mol$_{Ce}$ for $T \to 0$ is typical for the family of ternary $Ce_3M_4Sn_{13}$ compounds. At the low-T limit, however, C/T is strongly reduced when Sn is partially replaced by Sb atoms, while Co doping does not significantly change the high value of C/T. The $Ce_3Co_{4-x}Ru_xSn_{13}$ samples with $x \neq 0$ show, however, at about 3 K a clear Schottky contribution to C arising from the CEF scheme with small energy $\Delta_1 \approx 10$ K [24]. The insets to Figs. 10 and 11 display $C(T)$ at different magnetic fields. In order to estimate the characteristic Kondo temperature scale we adopted the resonant-level model as

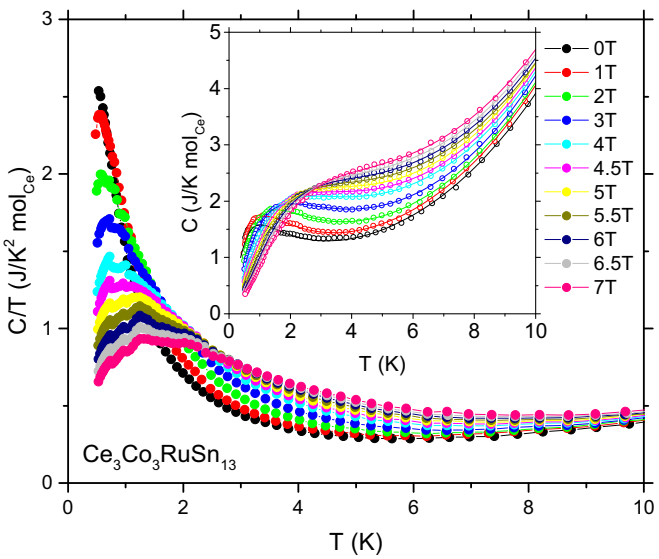

FIG. 11. $Ce_3Co_3RuSn_{13}$; $C(T)/T$ vs T for $Ce_3Co_3RuSn_{13}$ at different magnetic fields B. The inset shows $C(T)$ for different B [open points, plotted with the same colors as $C(T)/T$, respectively] and the fit of the resonance level model to the experimental data.

introduced by Schotte and Schotte [27]. This model assumes a narrow Lorentzian DOS at ϵ_F with a width $\Delta_K \sim T_K$, where T_K is the Kondo temperature. Within this model the Kondo-impurity contribution ΔC with effective spin $S = 1/2$ is described by the formula

$$\Delta C = k_B \frac{2S\Delta_K}{\pi k_B T} - 2k_B \times \mathrm{Re}\left\{\frac{(\Delta_K + ig\mu_B H)^2}{(2\pi k_B T)^2}\left[(2S+1)^2 \times \psi'\left(1 + \frac{\Delta_K + ig\mu_B H}{2\pi k_B T}(2S+1)\right) - \psi'\left(1 + \frac{\Delta_K + ig\mu_B H}{2\pi k_B T}\right)\right]\right\} \quad (2)$$

where ψ' is the first derivative of the digamma function, Δ_K/k_B is of the order of T_K, and R is the universal gas constant. A least-squares fit of expression $C(T) = \gamma_0 T + \beta T^3 + \Delta C$ to experimental data at $B = 0$ (cf. Figs. 10 and 11), together with the electron ($\gamma_0 T$) and phonon (βT^3) contributions gives $\Delta_K/k_B = 1.4$ K ($\gamma = 0.135$ J/K^2 mol$_{Ce}$, $\beta = 0.0023$ J/K^4 mol$_{Ce}$) for $Ce_3Co_3RuSn_{13}$ and $\Delta_K/k_B = 5.2$ K for $Ce_3Ru_4Sn_{12.35}Sb_{0.65}$ ($\gamma = 0.054$ J/K^2 mol$_{Ce}$, $\beta = 0.0006$ J/K^4 mol$_{Ce}$). Since the Kondo temperature $T_K \sim 1.5$ K has been characteristic of the known ternary $Ce_3M_4Sn_{13}$ systems, T_K of about 5 K seems to be unusual. Our XPS data and DFT calculations documented, however, an especially large value of the J_{cf} coupling constant for $Ce_3Ru_4Sn_{12.35}Sb_{0.65}$, three times larger than J_{cf} of the other samples listed in Table I, which correlates well with large Kondo temperature since $T_K \sim |J_{cf}N(\epsilon_F)|$. Extrapolation of the $\gamma_0 T + \beta T^3$ behavior yields a Sommerfeld coefficient $\gamma_0 = 0.656$ J/K^2 mol and Debye temperature $\theta_D = 200$ K for $Ce_3Ru_4Sn_{12.35}Sb_{0.65}$, and $\gamma_0 = 0.830$ J/K^2 mol and Debye temperature $\theta_D = 178$ K for $Ce_3Co_3RuSn_{13}$. The fitting parameter Δ_K is field dependent and increases with the magnetic field B; this behavior is

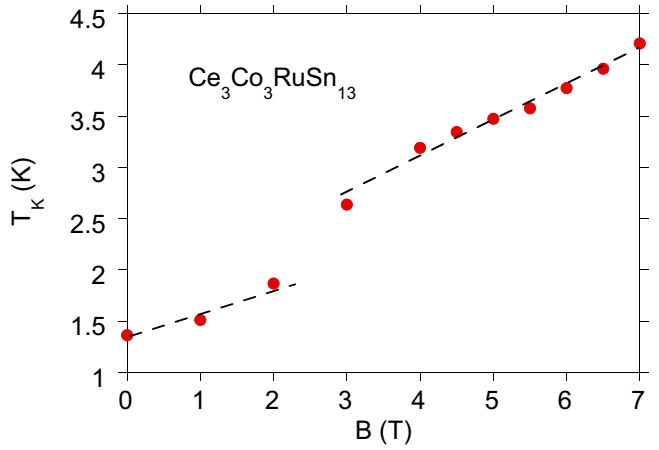

FIG. 13. Kondo temperature $T_K \equiv \Delta_K/k_B$ vs magnetic field for $Ce_3Co_3RuSn_{13}$ determined on the basis of the Kondo resonant-level model.

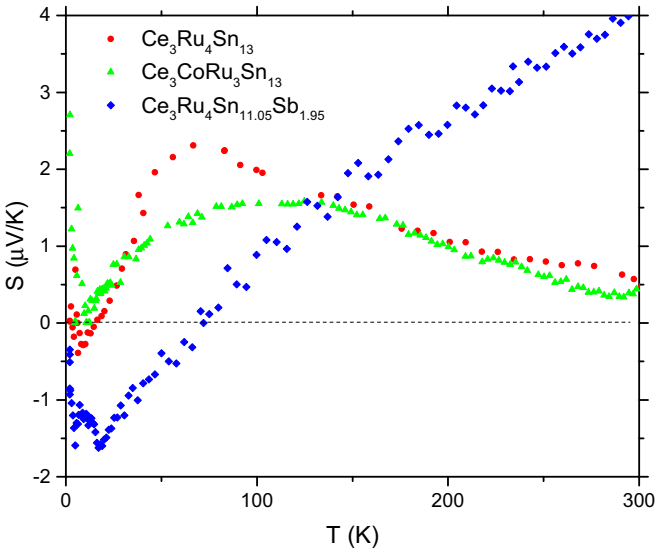

FIG. 14. Temperature-dependent thermopower S of $Ce_3Ru_4Sn_{13}$, $Ce_3Co_3RuSn_{13}$, and $Ce_3Ru_4Sn_{11.05}Sb_{1.95}$.

characteristic of the single-ion Kondo system [28]. In Fig. 13 the level width Δ_K/k_B of $Ce_3Co_3RuSn_{13}$ is found to increase with B from the value of 1.4 K ($B = 0$) to 4.2 K ($B = 7$ T). It is worth noting, however, a sharp change of T_K in the critical field of ~2.5 T. This unusual behavior suggests the field induced novel phase transition. Indeed, recent reports [5,24–26] have suggested $Ce_3Co_4Sn_{13}$ to be near a magnetic QCP. Namely, with increasing of B the system evolves from a magnetically correlated Kondo lattice state to a single-ion Kondo impurity state at about 2.5 T; however, in between these two regions a non-Fermi-liquid behavior has not been explicitly found [5]. A kink in the Δ_K/k_B versus B dependence shown in Fig. 13, also found in $Ce_3Ru_4Sn_{11.05}Sb_{1.95}$, signals such a field-induced phase transition between the magnetically correlated HF phase and the single-ion Kondo impurity state. Moreover, this field-induced transition does not depend on the type of dopant. It seems that the abnormal Δ_K/k_B versus B behavior is typical of the other isostructural $Ce_3M_4Sn_{13}$ stannides with the observed similar magnetic-field-dependent heat capacity as that displayed in Fig. 13, e.g., analogous field-induced phase transition has been recently documented for the series of $Ce_{3-x}La_xRh_4Sn_{13}$ and $x \geqslant 1$ compounds [16] with almost identical Δ_K/k_B versus B abnormal change at the field ~2.5 T. Recently, we have documented experimentally [16] that with increasing of the La doping the $Ce_{3-x}La_xRh_4Sn_{13}$ system evolves from magnetically correlated HF state to a single-ion Kondo impurity state near the critical concentration $x_c \sim 1$.

C. Thermoelectric properties of Sb- and Co-doped $Ce_3Ru_4Sn_{13}$

The Seebeck coefficient $S(T)$ of $Ce_3Ru_4Sn_{13}$, $Ce_3Co_3RuSn_{13}$, and $Ce_3Ru_4Sn_{11.05}Sb_{1.95}$ is displayed in Fig. 14. The absolute values of S are much smaller than those expected for strongly electron correlated material. Around 80 K ($Ce_3Ru_4Sn_{13}$) and 130 K ($Ce_3Co_3RuSn_{13}$) the thermopower exhibits a broad peak, which may be caused by the CEF splitting of the Ce^{3+} ground state. Then the total CEF splitting Δ_{CEF} is estimated to be about 240 or 390 K, respectively, as scattering from an excited level of Ce^{3+} generates a positive contribution to S with a maximum at about $\Delta_{CEF}/3k_B$ [29]. This simple estimate of the CEF structure also gives satisfactory description of the magnetic susceptibility and specific heat for both compounds. Common to these compounds is a minimum at about 10 K with negative thermopower and at elevated temperatures a crossover to positive value. The positive $S(T)$ values signify that hole-type carriers dominate thermoelectric transport. Actually in $Ce_3Co_4Sn_{13}$ and $Ce_3Ru_4Sn_{13}$ the bands form the holelike Fermi surface along $\Gamma - R - M$, $\Gamma - M$, and $X - M$ directions [17], which can contribute to heat transport properties. The largest positive values of S observed at $T = 2$ K are attributed to Kondo-type interaction that is reflected by the large C/T value below $T_K \approx 1.5$ K. The

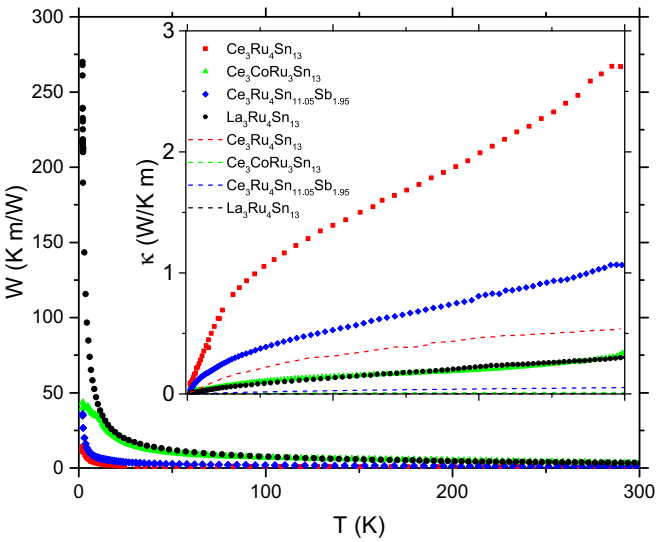

FIG. 15. Thermal resistivity W and thermal conductivity κ (inset) for $Ce_3Ru_4Sn_{13}$, $La_3Ru_4Sn_{13}$, $Ce_3Co_3RuSn_{13}$, and $Ce_3Ru_4Sn_{11.05}Sb_{1.95}$ in temperature range 2 and 300 K. The calculated electron thermal conductivity is represented by the dotted lines.

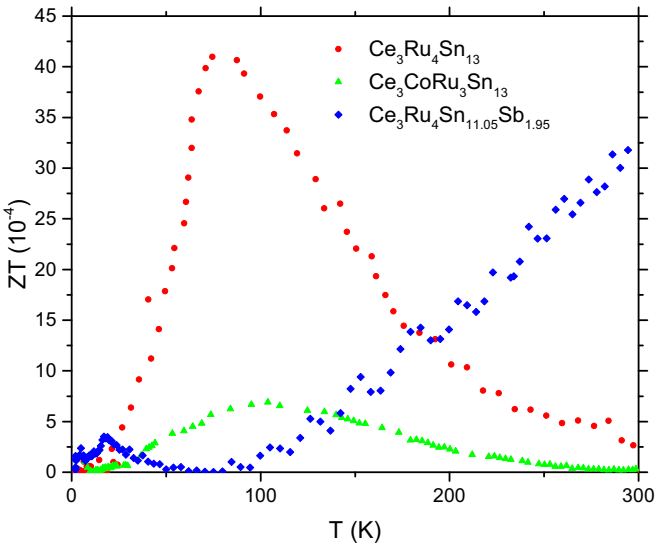

FIG. 16. The *figure of merit* for $Ce_3Ru_4Sn_{13}$, $Ce_3Co_3RuSn_{13}$, and $Ce_3Ru_4Sn_{11.05}Sb_{1.95}$.

Seebeck coefficient of the Sb-doped $Ce_3Ru_4Sn_{11.05}Sb_{1.95}$ sample also shows similar crossover to positive value at ∼80 K upon heating, and S increases linearly with temperature, which is typical for metals; however, it does not show any feature resulting from CEF effect. Figure 15 shows the temperature-dependent thermal conductivity κ and thermal resistivity W for $Ce_3Ru_4Sn_{13}$, $La_3Ru_4Sn_{13}$, $Ce_3Co_3RuSn_{13}$, and $Ce_3Ru_4Sn_{11.05}Sb_{1.95}$, respectively. The value of both quantities varies with doping. Taking into account the Wiedemann-Franz law, the total thermal conductivity $\kappa(T)$ can be separated into the electronic part κ_e and the lattice part κ_{ph}. Results are presented in Fig. 15 as solid and dotted lines for κ_{ph} and κ_e, respectively. A good thermoelectric material needs total κ as small as possible; this is, however, not the case. There are several reasons to explain a relatively good thermal conductivity in these materials. The most significant is the effect of rattling atoms strongly (or completely) reduced by the strong covalent bonds inside the $Sn1(Sn2)_{12}$ and $Ce(Sn2)_{12}$ cages (see Sec. III B, also [8,16]). Moreover, the effective heat transport scattering mechanism increases with alloying, which leads to similar decrease of total κ with doping of $Ce_3Ru_4Sn_{13}$ by Co or Sb. However, comparing $\kappa(T)$ of the doped $Ce_3Ru_3CoSn_{13}$ with that of the analogous nonmagnetic $La_3Ru_4Sn_{13}$ reveals similar values of both; this suggests also the additional process of scattering of the charge carriers on the Ce magnetic ions in the disordered lattice. The estimate reveals that the phonon thermal conductivity is much larger than the electron one. The very low values of electronic conduction of heat, clearly visible for the doped $Ce_3Ru_3CoSn_{13}$, can be associated with an effective scattering mechanism impeding the heat transport of electrons, and/or with a low DOS at the Fermi energy (see Table I). Figure 16 exhibits the calculated *figure of merit* in temperature range 2 and 300 K, which is much smaller than expected [10,31,32] for the family of the $Ce_3M_4Sn_{13}$ filled cage compounds. We also found that granulation does not effect ZT [30] much. The materials considered for thermoelectric application should exhibit value for the *figure of merit* $ZT = S^2T/(\kappa\rho)$ at least of the order of 1 (ρ is electrical resistivity).

IV. CONCLUDING REMARKS

The present study shows that the ground-state properties of $Ce_3Ru_4Sn_{13}$ are substantially determined by crystal electric-field splitting of the $J = 5/2$ total angular momentum. The susceptibility can be well described in terms of the CEF model considering the tetragonal Ce point symmetry, where the J multiplet of the Ce ion splits into three doublets with the low-lying one first, about $\Delta_1 \approx 10$ K above the ground-state level. The structural deformation of the $Sn2_{12}$ cages as a result of strong covalent bonding between Sn2 and atom M evidently correlates with asymmetry in shape of the Sn $4d$ core-level XPS spectra. The evidence for the covalent bondings from experiment and electronic band-structure calculations strongly determines the poor thermoelectric properties of the family of $R_3M_4Sn_{13}$ skutterudite-related materials.

The Kondo temperature T_K has been obtained as ∼1.5 K for most of the ternary $Ce_3M_4Sn_{13}$ compounds. We found that the doping does not change T_K significantly, excluding the case of $Ce_3Ru_4Sn_{12.35}Sb_{0.65}$, where the value of the DOS at the Fermi level is calculated almost twice larger, which results in much stronger Kondo coupling with $T_K \sim 5$ K. On the basis of complementary investigations supplemented by the band-structure calculations we explained the impact of doping on the magnetic susceptibility of $Ce_3Ru_xCo_{4-x}Sn_{13}$ and $Ce_3Ru_4Sn_{13-x}Sb_x$. Namely, doping with Sb atoms practically does not change $\chi(T)$, while in $Ce_3Co_{4-x}Ru_xSn_{13}$ magnetic susceptibility strongly depends on the amount of Co, and the Pauli paramagnetic contribution to χ is measured one order of magnitude larger.

An interesting observation is the novel field-induced phase transition between the magnetically correlated HF phase and the single-ion Kondo impurity state in $Ce_3Ru_4Sn_{13}$, previously suggested for $Ce_3Co_4Sn_{13}$ [5]. We have shown that this field-induced transition does not depend on the type of dopant.

Literature data have not shown yet a significant thermoelectric effect for most of the known $Ce_3M_4Sn_{13}$ compounds. We found the poor thermoelectric characteristics of $Ce_3Ru_4Sn_{13}$ and confirmed that the doping can only slightly increase ZT value, but the effect is not significant.

ACKNOWLEDGMENTS

We thank National Science Centre (NCN) for financial support, on the basis of Decision No. DEC-2012/07/B/ST3/03027. L.K. thanks NCN (Poland) for financial support, on the basis of Decision No. DEC-2014/15/N/ST3/03799. P.W. thanks NCN (Poland) for financial support, on the basis of Decision No. DEC-2015/17/N/ST3/02361.

[1] See special issue of J. Phys.: Condens. Matter **8**, 48 (1996) (edited by P. Coleman, M. B. Maple, and A. Millis).

[2] A. Ślebarski, M. Fijałkowski, M. M. Maśka, M. Mierzejewski, B. D. White, and M. B. Maple, Phys. Rev. B **89**, 125111 (2014).

[3] L. E. Klintberg, S. K. Goh, P. L. Alireza, P. J. Saines, D. A. Tompsett, P. W. Logg, J. Yang, B. Chen, K. Yoshimura, and F. M. Grosche, Phys. Rev. Lett. **109**, 237008 (2012).

[4] E. L. Thomas, H.-O. Lee, A. N. Bonkston, S. MaQuilon, P. Klavins, M. Moldovan, D. P. Young, Z. Fisk, and J. Y. Chan, J. Sol. State Chem. **179**, 1642 (2006).

[5] A. L. Cornelius, A. D. Christianson, J. L. Lawrence, V. Fritsch, E. D. Bauer, J. L. Sarrao, J. D. Thompson, and P. G. Pagliuso, Physica B **378–380**, 113 (2006).

[6] A. Ślebarski, M. Fijałkowski, J. Goraus, L. Kalinowski, and P. Witas, J. Alloys Compds. **615**, 921 (2014).

[7] S. K. Goh, D. A. Tompsett, P. J. Saines, H. C. Chang, T. Matsumoto, M. Imai, K. Yoshimura, and F. M. Grosche, Phys. Rev. Lett. **114**, 097002 (2015).

[8] A. Ślebarski, J. Goraus, P. Witas, L. Kalinowski, and M. Fijałkowski, Phys. Rev. B **91**, 035101 (2015).

[9] Clear evidence has been found for isoelectronic substitution of Sr occupying *R* atomic sites by Ca, with effect of applying chemical pressure [7].

[10] H. Luo, J. W. Krizan, L. Muechler, N. Haldolaarachchige, T. Klimczuk, W. Xie, M. K. Fuccillo, C. Felser, and R. J. Cava, Nat. Commun. **6**, 6489 (2015).

[11] J. P. Remeika, G. P. Espinosa, A. S. Cooper, H. Barz, J. M. Rowel, D. B. McWhan, J. M. Vandenberg, D. E. Moncton, Z. Fizk, L. D. Woolf, H. C. Hamaker, M. B. Maple, G. Shirane, and W. Thomlinson, Sol. State Commun. **34**, 923 (1980); J. L. Hodeau, M. Marezio, J. P. Remeika, and C. H. Chen, *ibid.* **42**, 97 (1982).

[12] K. Koepernik and H. Eschrig, Phys. Rev. B **59**, 1743 (1999); I. Opahle, K. Koepernik, and H. Eschrig, *ibid.* **60**, 14035 (1999); K. Koepernik, B. Velicky, R. Hayn, and H. Eschrig, *ibid.* **55**, 5717 (1997); H. Eschrig, K. Koepernik, and I. Chaplygin, J. Solid State Chem. **176**, 482 (2003); www.fplo.de

[13] Computer code ELK FP-LAPW code, version 3.1.12, http://elk.sourceforge.net/.

[14] J. P. Perdew and Y. Wang, Phys. Rev. B **45**, 13244 (1992).

[15] A. Ślebarski and J. Goraus, Phys. Rev. B **88**, 155122 (2013).

[16] A. Ślebarski, P. Witas, J. Goraus, L. Kalinowski, and M. Fijałkowski, Phys. Rev. B **90**, 075123 (2014).

[17] A. Ślebarski, J. Goraus, and P. Witas, Phys. Rev. B **92**, 155136 (2015).

[18] O. Gunnarsson and K. Schönhammer, Phys. Rev. B **28**, 4315 (1983); J. C. Fuggle, F. U. Hillebrecht, Z. Zolnierek, R. Lässer, Ch. Freiburg, O. Gunnarsson, and K. Schönhammer, *ibid.* **27**, 7330 (1983).

[19] A. Ślebarski, T. Zawada, J. Spałek, and A. Jezierski, Phys. Rev. B **70**, 235112 (2004).

[20] P. W. Anderson, Phys. Rev. **124**, 41 (1961).

[21] Y. Baer and Ch. Zürcher, Phys. Rev. Lett. **39**, 956 (1977); Y. Baer, R. Hauger, Ch. Zürcher, M. Campagna, and G. K. Wertheim, Phys. Rev. B **18**, 4433 (1978).

[22] J. R. Schrieffer and P. A. Wolff, Phys. Rev. **149**, 491 (1966).

[23] J. Mulak, J. Less Common Met. **121**, 141 (1986).

[24] The CEF effect in $Ce_3Ru_4Sn_{13}$ parent compound was recently discussed in [6]. In contrast, the low-T Schottky anomaly has not been observed in the specific-heat data of $Ce_3Co_4Sn_{13}$ [5,25,26]. However, $Ce_3Co_4Sn_{13}$ shows a crossover from magnetically correlated state with large value of $C/T \sim 4\ \mathrm{J/K^2\ mol_{Ce}}$ to a single impurity state in applied magnetic fields of about 2.5 T. The magnetic correlations are not strong enough to promote long-range order.

[25] D. T. Adroja, A. M. Strydom, A. P. Murani, W. A. Kockelmann, and A. Fraile, Physica B **403**, 898 (2008).

[26] A. D. Christianson, E. A. Goremychkin, J. S. Gardner, H. J. Kang, J.-H. Chung, P. Manuel, J. D. Thompson, J. L. Sarrao, and J. M. Lawrence, Physica B **403**, 909 (2008).

[27] K. D. Schotte and U. Schotte, Phys. Lett. **55**, 38 (1975).

[28] P. D. Sacramento and P. Schlottmann, Phys. Rev. B **40**, 431 (1989).

[29] A. K. Bhattacharjee and B. Coqblin, Phys. Rev. B **13**, 3441 (1976).

[30] P. Witas, L. Kalinowski, J. Goraus, M. Fijałkowski, and A. Ślebarski, Acta Phys. Polon. A **127**, 309 (2015).

[31] B. C. Sales, B. D. Mandrus, and R. K. William, Science **272**, 1325 (1996).

[32] G. D. Mahan, B. C. Sales, and J. W. Sharp, Phys. Today **50**, 42 (1997).